

## Novel Dynamic Model to Predict the Glycosylation Pattern of Monoclonal Antibodies from Extracellular Cell Culture Conditions

Ohadi Kaveh\* Aghamohseni Hengameh\*\*  
Gädke Johannes\*\*\* Moo-Young Murray\*\*\*\* Legge Raymond L.\*\*\*\*\*  
Scharer Jen\*\*\*\*\* Budman Hector M.\*\*\*\*\*

Chemical Engineering Department, University of Waterloo, Waterloo, Ontario, Canada

\* e-mail: skohadi@uwaterloo.ca, \*\* e-mail: h3aghamo@uwaterloo.ca,

\*\*\* e-mail: j.gaedke@tu-bs.de, \*\*\*\* e-mail: mooyoung@uwaterloo.ca, \*\*\*\*\* e-mail: rllgge@uwaterloo.ca

\*\*\*\*\* e-mail: jscharer@uwaterloo.ca, \*\*\*\*\* e-mail: hbudman@uwaterloo.ca

**Abstract:** Glycosylation is a critical protein post-translational modification with a profound impact on the therapeutic properties of Mab and research indicates that it depends on extracellular culture conditions. A novel dynamic model was developed to relate extracellular metabolites' concentrations to a cumulative glycoprofile. The model has three components: dynamic evolution of extracellular metabolites, production of nucleotide sugars in the cytosol, and glycosylation inside the Golgi apparatus. Following comparisons with experimental data obtained from batch CHO cell cultures, the model was found capable of predicting the glycoform profile of Mab temporally, as well as the extent of galactosylation given in the form of galactosylation index. The model has the potential for use in controlling the glycoform profile by manipulating culture conditions.

**Keywords:** Dynamic modeling, Biotechnology, Glycosylation Mammalian cell culture Monoclonal antibody

### 1. INTRODUCTION

Monoclonal antibodies (Mabs) comprise the dominant products in the fastest growing segment of the biopharmaceutical market. Chinese hamster ovary (CHO) cells are widely used as hosts for Mab production. Several studies have reported the profound impact of glycosylation, as post-translational modification, on Mabs' therapeutic properties. The degree and extent of glycosylation can be quantified in terms of the type and number of nucleotide sugars attached to the Mab (Durocher and Butler, 2009).

N-linked glycosylation, the most common form of glycosylation in mammalian cells, is initiated in the endoplasmic reticulum (ER) by a covalent attachment of a sugar to the polypeptide chain that is followed by proper folding of the protein and removal of three glucose molecules and at least one mannose. The resulting glycoprotein is then transferred into the Golgi apparatus where the final glycosylation process takes place (Del Val et al., 2011, Hossler et al., 2007, Stanley, 2011).

It has been reported (Del Val et al., 2011, Hossler et al., 2009) and experimentally observed by the authors that culture conditions can be manipulated to obtain a specific oligosaccharide (OS) structure attached to the Mab. Accordingly, a mathematical model that could describe the effect of culture conditions on glycosylation may be instrumental for manufacturing a Mab with a desired glycoprofile. Such a model should be able to relate the extracellular culture conditions to intracellular glycosylation mechanisms at the cell level. To the knowledge of the authors, no such model has yet been developed.

Quality by Design (QbD) is a recent FDA initiative that promotes a systematic approach to drug development, emphasizing that product quality considerations should be introduced at the design stage of the manufacturing process. Predictive mathematical models, such as the one proposed in this study, have been identified as key for designing novel manufacturing operations within the QbD framework (Hossler et al., 2009).

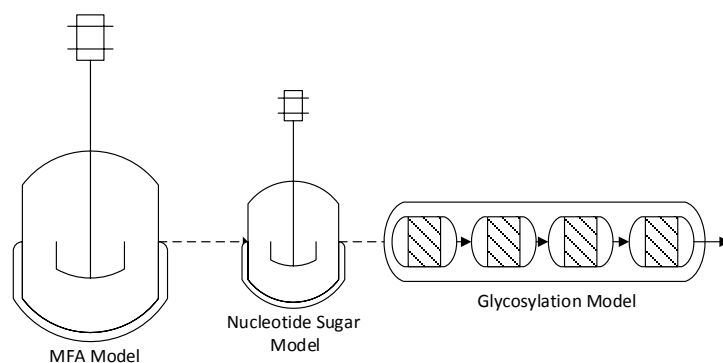


Fig. 1. Schematic representation of the comprehensive-model: Metabolic Flux Analysis (left), Nucleotide Sugar (centre), Glycosylation based on Golgi Maturation (right).

In the current work a specifically engineered CHO cell line, provided by MabNet (National Science and Engineering Research of Canada Mab Network), has been used to produce glycosylated Mab. A comprehensive model is developed for this cell line that is composed of three main parts as shown in Fig. 1. The first part consisting of a metabolic flux analysis (MFA) based model is developed to describe changes in

extracellular metabolites concentrations. The second part bridges the gap between metabolite uptake and glycosylation in the Golgi apparatus. This part, shown by the middle block in Fig. 1, involves modelling the synthesis of the essential nucleotide sugars from glucose and glutamine in the cytosol (or the nucleus for CMP-Neu5Ac). In the third part, to the right of Fig. 1, the glycosylation inside the Golgi apparatus is mathematically modelled based on the Golgi maturation assumption (Del Val et al., 2011, Hossler et al., 2007). Since many of the parameters of three parts of the model have not been explicitly documented in the literature or they have not been reported for the specific cell line under consideration, a comprehensive sensitivity analysis with respect to parameters was conducted based on experimental results to identify which parameters are more critical for model calibration. Preliminary model calibration was done with data for extracellular metabolites' concentrations and glycosylation pattern at different days of the cell cultures. It should, be emphasized that while the first block in Fig. 1 is used to describe average extracellular metabolites' concentration in the culture media, the third block of the model describes glycosylation at the intracellular level. Since samples were collected at different days of culture, the glycoprofiles reported in this work reflect a cumulative time average of producing cells undergoing glycosylation under varying culture conditions. Consequently, as further explained in the following sections, for comparing model predictions with measurements, it was required to translate the intracellular OS concentration values, calculated by the third component shown in Fig. 1, to a cumulative average value over culture time based on the instantaneous Mab productivity along the time course of the culture. The subsequent sections describe the experimental techniques followed by theoretical details about the mathematical model and comparisons of model predictions with experimental data.

## 2. MATERIALS AND METHODS

### 2.1 Culture Condition

The cell line used in the present study is a CHO cell line derived from the parental CHO-DXB11 cell line, specifically engineered and provided by MabNet expressing the EG2-hFc, a camelid Mab. The cells were maintained in regular serum free Biogro medium (Provided by MabNet) supplemented with 0.9 % HT (Invitrogen:11067-030). Seed cultures were produced by sub-culturing the cells every 2 to 3 days with a seeding density of 0.25 million cells/ml. Cultures were grown in 500 ml polycarbonate shake-flasks with 250 ml working volume at initial cell density of 0.2 million cell/ml. Flasks were agitated at 120 rpm, and incubated at 37°C with 5% CO<sub>2</sub>. Batch experiments were performed at initial glucose concentration of 25 mM at different levels of initial glutamine concentration (0 and 4 mM). A glucose concentration of 25 mM was found to be optimal for growth. Samples were taken on daily basis for *at situ* analysis of viable and dead cell concentration using trypan-blue exclusion method. In addition, samples were collected,

centrifuged at 300×g for 10 minutes, and their supernatant were stored at -20°C to perform off-line measurements.

### 2.2 Analytical Methods

Enzyme-Linked Immunosorbent Assay (ELISA) method, developed by MabNet, was applied to obtain recombinant protein concentration. The Mab concentration was calculated conventionally by comparing the optical density of each sample with the standard curve.

Glucose, glutamine, lactate, and ammonia concentration of culture broth were measured using a multi-parameter bioanalytical system, Bioprofile 400 (Nova Biomedical, Waltham, MA), off-line.

In order to obtain the composition of the glycans/OSs attached to Mab, a hydrophilic interaction chromatography, following by an exoglycosidase enzyme array digestion method was implemented (Brockhausen, 2006). This analysis was performed on samples obtained every other day, starting from the third day of the culture.

## 3. MODEL DEVELOPMENT

The development of the dynamic metabolic flux equations commenced with a detailed steady state flux analysis for this CHO line using the procedure described previously (Naderi et al., 2011). An important conclusion of the flux balance analysis, not shown here for brevity, was that all non-essential amino acid synthesis could be described in terms of co-metabolism of glucose [*glc*] and glutamine [*gln*]. Obviously, this co-metabolism also affects biomass ( $X_v$ ) and ultimately Mab synthesis as well.

The viable biomass population is differentiated as growing (*fgr*) and a non-growing ( $1 - fgr$ ) fraction. The non-growing fraction includes both resting cells arrested in the G phase as well as apoptotic cells. In our previous study (Naderi et al., 2011) these two sub-populations were modelled separately. However, in the present case no significant differences in either metabolite uptake or Mab productivity were observed to necessitate separation. Consequently the dynamic model for cell growth is as (1).

$$\frac{dX_v}{dt} = \mu fgr X_v - k_d (1 - fgr) X_v \frac{1}{1 + K_{11} e^{-\frac{[N]}{K_{12}}}} \quad (1)$$

Where  $\mu$  is specific growth rate,  $k_d$  is specific death rate and  $K_{ij}$ s are model parameters. As in case of our previous models (Naderi et al., 2011) the rate of death is enhanced by the ammonia concentration, [N]. The total ammonia concentration, in turn, was calculated from the metabolic flux balance equations (not shown here).

The estimation of the temporal dependence of the growing cell fraction is a key aspect of the model. A number of plausible model structures were considered and the following choice was made by invoking Akaike's information criterion for model selection (Burnham and Anderson, 2002) using a

comparison of predicted versus simulated total viable biomass concentration, being formulated as (2).

$$\frac{dfgr}{dt} = -K_{21} \frac{fgr}{1 + [glc][gln]/K_{22}} \quad (2)$$

Equation (2) simulates the dependence of the observed growth rate on the product of the glutamine and glucose concentration. Also, as observed experimentally, the growth did not stop immediately if either glucose or glutamine were exhausted from the medium.

The dynamic metabolic flux models for glucose and glutamine metabolism are shown in (3) and (4) respectively.

$$\frac{d[glc]}{dt} = -K_{31} fgr X_v \frac{[glc][gln]}{K_{32} + [glc][gln]} - K_{33} X_v \quad (3)$$

$$\frac{d[gln]}{dt} = -K_{41} fgr X_v \frac{[glc][gln]}{K_{42} + [glc][gln]} - K_{43} X_v \quad (4)$$

As shown above, both glucose and glutamine metabolism consists of growth associated and a non-growth associated terms. Glucose and glutamine appear to be co-metabolized. It is noteworthy that an identical half-saturation constant for the co-metabolism ( $K_{32}$  and  $K_{42}$ ) satisfied both equations (15.77 mM<sup>2</sup>).

The selection of a robust model that adequately describes the system requires careful examination of the parameter values. The parameter values (not shown for brevity) and their distributions in this study were generated by the Gibbs sampler version of the Metropolis-Hastings algorithm (Jitjareonchai et al., 2006). Markov Chain Monte Carlo (MCMC) methods such as the Metropolis-Hastings algorithm used here have been proven to be powerful tools, especially when some prior knowledge about the parameters is available from the literature.

The middle block in Fig. 1 consists of a simplified model to simulate the production of nucleotide sugars from glucose and glutamine in the cytosol (or nucleus for CMP-Neu5Ac). This model is formulated to connect between the extracellular metabolites' concentration and the glycoform profile of produced MAb. Fig. 2 exhibits the simplified reaction network connecting the extracellular glucose and glutamine concentrations to nucleotide sugars based on the database Kyoto Encyclopaedia of Genes and Genomes (KEGG) where the intermediate reactions are lumped together for simplicity (Kanehisa and Goto, 2000, Kanehisa et al., 2012). The amount of glucose and glutamine being consumed towards the production of nucleotide sugar is negligible compared to the consumption of these nutrients towards cell growth and maintenance. Thus this consumption (Fig 2) is not included in the MFA model. The reaction rates are assumed to be irreversible following a one or two-substrate Michaelis-Menten kinetics, as shown in (6). Additionally, a first order dissociation kinetic rate is utilized to depict the dissociation of nucleotide sugars following their incorporation into biomass production. The mass balance for each of the

nucleotide sugars is given in general form by (5), assuming that the cytosol (or nucleus) acts as an ideal batch reactor. The model uses the extracellular glucose and glutamine concentration and accounts for the mass transfer across the cell membranes through the calibrated parameters.

$$\frac{d[Sug]_i^{Cyt}}{dt} = \sum v_i r_i^{Cyt} - K_{[Sug]}^{dissociation} [Sug]_i^{Cyt} \quad (5)$$

$$r_i^{Cyt} = \frac{[Sug]_p^{Cyt} [Sug]_q^{Cyt}}{(K_p + [Sug]_p^{Cyt})(K_q + [Sug]_q^{Cyt})} \quad (6)$$

Although the glycosylation starts in the ER, in the current study it is assumed that the proteins are properly folded in ER and only contain nine-mannose attached to their constant heavy chain. Thus the glycosylation model, represented by the rightmost block in Fig. 1, simulates the transfer of nucleotide sugars inside the Golgi only. In the Golgi, a few numbers of enzymes will catalyse a large number of sequential reactions that shift the high mannose structure of the saccharide exiting the ER towards complex and hybrid conformations; hence, each enzyme can trigger various reactions (Del Val et al., 2011, Hossler et al., 2007, Stanley, 2011). This large network of reactions has been mathematically described in a form of *relationship-matrix* by Hossler, et al, 2007. Previous studies have reported that the Golgi apparatus, consisting of four different cisternae, can be approximated as if each compartment converts to a successive one through a maturation procedure (cisternal maturation). Consequently, and following (Del Val et al., 2011, Hossler et al., 2007) in this study the Golgi was represented by four ideal (no radial and axial dispersion) plug flow reactors (PFR) in series, each representing one cisterna, at steady state conditions. Different overall retention time in the Golgi has been assumed in literature. In this work the overall residence time of Golgi (all four compartments) is set to be forty minutes as postulated in Hossler et al. 2007.

The glycosylation reactions occurring in the Golgi are catalyzed by two main groups of enzymes: exoglycosidases and glycosyl-transferases (GTs) (Del Val et al., 2011, Hossler et al., 2007, Stanley, 2011). For simplicity, exoglycosidases were assumed to follow irreversible one-substrate Michaelis-Menten kinetic showed in (7) while the GTs follow irreversible two-substrate kinetic, as shown in (8) (Hossler et al., 2007). It is worth mentioning that GTs were assumed to have only one functional group and each can only transfer an specific nucleotide sugar (Stanley, 2011).

The superscript  $n$  specifies the compartment/cistern number,  $k$  determines the corresponding enzyme and its nucleotide sugar (for GTs). The  $\alpha$ -s in (7) and (8) are coefficients that define the spatial distribution of enzymes along the Golgi compartments (Hossler et al., 2007, Stanley, 2011). Thus, they can determine the direction along the network of reactions. Kinetic parameters presented in (7) and (8) strongly depend on the cell line, thus different values are reported in literature. In this work  $K_k^G$ ,  $K_k^S$ , and  $r_k^{max}$  values

were selected as per the values documented by Hossler, et al, 2007.

$$r_k^n = \frac{\alpha_k^n r_k^{\max} [Glyc_i]^n}{K_k^G (1 + \sum_{z=1}^{NC} \frac{[Glyc_z]^n}{K_k^G})} \quad (7)$$

$$r_k^n = \frac{\alpha_k^n r_k^{\max} [Glyc_i]^n [Sug_k]^n}{K_k^G (1 + \sum_{z=1}^{NC} \frac{[Glyc_z]^n}{K_k^G} + \frac{[Sug_k]^n}{K_k^S} + \sum_{z=1}^{NC} \frac{[Glyc_z]^n [Sug_k]^n}{K_k^G K_k^S})} \quad (8)$$

Concentration of 9-Mannose, UDP-Gal, UDP-GlcNAc, GDP-Fuc, and CMP-Sia (Neu5Ac), depend on the extra cellular availability of glucose and glutamine. After being produced in the cytosol (or the nucleus), these sugars are fed into the Golgi apparatus.

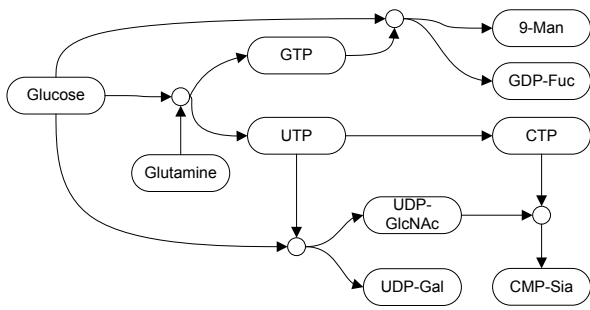


Fig. 2. Simplified reaction-tree of nucleotide sugars inside the cytosol (or nucleus). Man: mannose, Gal: galactose, GlcNAc: N-acetylglucosamine, Fuc: Fucose, Sia: sialic acid.

The glycosylation model, as presented in previous studies (Del Val et al., 2011, Hossler et al., 2007), depict the instantaneous OS pattern of the Golgi in one individual cell. However, the experimental results provide a cumulative average of the glycosylated Mab accumulated in the supernatant over the time of the culture up to the time of the measurement. To account for this effect, (9) was utilized to convert the instantaneous glycan composition calculated as per Golgi maturation model to the accumulated one measured experimentally.

$$[Glyc_i]^{Acc} = \frac{\int_0^t \dot{Mab} [Glyc_i]^{Ins} dt}{\int_0^t \dot{Mab} dt} \quad (9)$$

For the purpose of comparisons and for simplicity it was hypothesized that the experimental glycan composition at day three is identical to the instantaneous OS composition at the beginning of the culture. This claim can be supported by the fact that a negligible amount of glycoprotein was measured during the first three days of the culture. For the purpose of model calibration, the  $\alpha$ -s were obtained by minimizing the sum of square error (SSE) of OSs using genetic algorithm (GA), while the nucleotide sugars were assumed to be in excess (at the beginning of the culture). The nucleotide-sugar

model's parameters were calibrated by minimizing the SSE between comprehensive-model predictions and measured glycoprofiles along the culture time, using data from the batch with no glutamine added to it initially.

In order to simplify the quantification of glycosylation extent, the relative abundance area of predominant glycan structures can be lumped together in a form of glycosylation indices: galactosylation index (GI), sialiation index (SI), and fucosylation index (FI). However, the focus of current work is on GI since this cell line is highly galactosylated. The agalactosylated ( $G_i^0$ ), monogalactosylated ( $G_i^1$ ), and digalactosylated ( $G_i^2$ ) OSs were lumped within the GI as shown by (10). This grouping is further motivated by the fact that the therapeutic properties of Mabs have been often correlated to these indices (Majid et al., 2007).

$$GI = \frac{\sum_i G_i^2 + 0.5 \times \sum_i G_i^1}{\sum_i G_i^2 + \sum_i G_i^1 + \sum_i G_i^0} \quad (10)$$

Due the high number of OSs proposed in Hosslet et al. 2007 (341 OSs), the computation is very costly. To reduce computations, the large network of reactions was trimmed based on the experimental data, to encompass only the plausible Mab's OSs for this particular cell line. At current stage the model solves the mass balance equations for 100 OSs and four nucleotide sugars inside the Golg apparatus. This has significantly reduced the run time as compared to the original model. To further decrease the CPU time, conditional statements were avoided. By perusing the matrix calculation and use of binary matrices, instead of conditional statements, the CPU time was drastically reduced. Additionally, the program was modified to take advantage of parallel computation toolbox in MATLAB that reduced the run time by 1/10. On a hex-core Intel CPU computer equipped with 16 gigabyte of RAM, it takes approximately 30 seconds to run the program for simulating 9 days of culture.

#### 4. RESULTS AND DISCUSSION

The simulations of the viable cell concentration with 4 and 0 mM glutamine added is shown in Fig. 3 This particular CHO cell line is relatively fast growing, having a minimum generation time of approximately 16.5 hours. With 4 mM glutamine initially, a maximal viable cell density of over 3.7 million cells/ml is reached after 5 days of incubation. In contrast, the maximum cell density when no glutamine is added to the medium is about one-half of that obtained with the 4 mM.

The model slightly underestimates the viable cell density concentration for the culture when no glutamine is added. It should be emphasized that the 0 mM glutamine experiments have not been used for model calibration so as to test the predictive capabilities of the model. Although the culture commencing with 4mM glutamine reaches a higher viable cell concentration, the viability drops sharply after day five. This is probably due to the glucose concentration being

depleted more quickly, compared to the culture with no glutamine added at the beginning (Fig. 4).

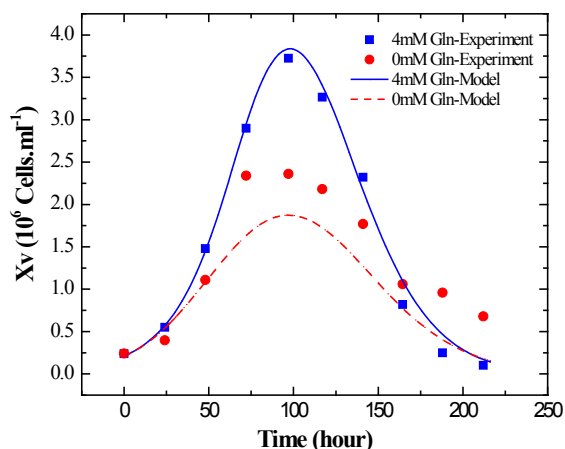


Fig. 3. Viable cell concentration time profile of two different batch cultures; simulated vs. experimental.

The time profiles of the extracellular glucose and glutamine concentrations are shown in Fig. 4 and Fig. 5, respectively. With 4 mM glutamine present initially, glutamine exhaustion coincided with the maximum cell concentration. Glucose was exhausted somewhat later, after 6 days of culture.

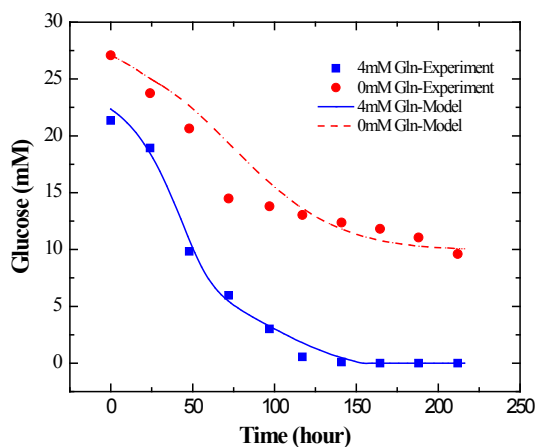


Fig. 4. Extracellular glucose concentration time profile of two different batch cultures; simulated vs. experimental.

When no glutamine is added, the initial glutamine concentration reflects the residual concentration introduced with the inoculum. In this case, glutamine is rapidly consumed and after 2 days it is below detection limits. It is noteworthy that the minimum measurement threshold of the bioprofile for glutamine is 0.2 mM. Due to the observed co-metabolism of glutamine and glucose, glycosylation was expected to stop after glutamine depletion. However, in reality glycosylation continued after the point that glutamine fell below a non-detectable amount. Accordingly, it was necessary to assume a nonzero intracellular glutamine concentration beyond this point possibly indicating that glutamine is consumed at very slow rates at low

concentrations. On the other hand, beyond that point, the glucose concentration was consumed at a much slower rate and significant concentrations were observed and predicted even after nine days of culture. This can be attributed to the co-metabolism with glutamine.

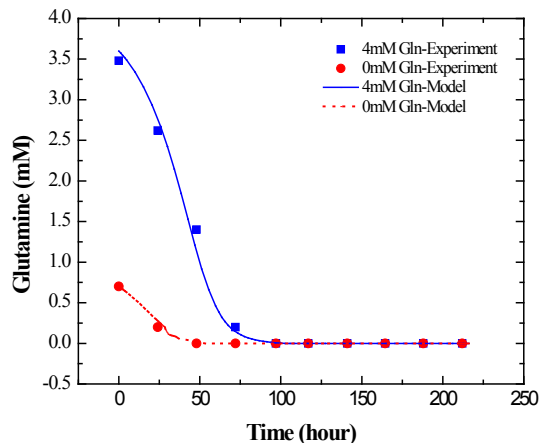


Fig. 5. Extracellular glutamine concentration time profile of two different batch cultures; simulated vs. experimental.

Based on the experimental results (not shown), it can be concluded that this cell line produces a highly galactosylated Mab. The concentration of nucleotide sugars was found to be strongly correlated with glucose and glutamine concentrations. Following the parameter estimation exercise, explained in the previous section, the model was found to be less sensitive to the glutamine compared to the glucose concentration.

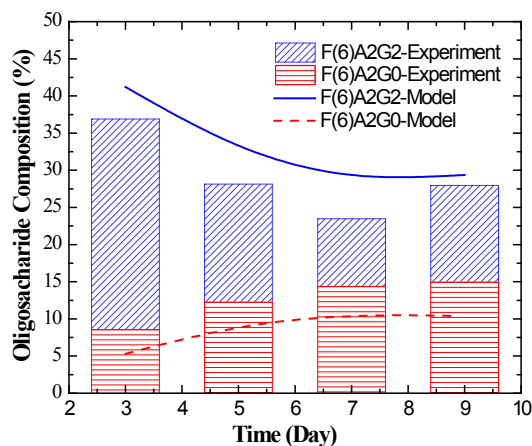


Fig. 6. Time profile of simulated and measured cumulative oligosaccharides (F(6)A2G0 and F(6)A2G2) concentrations for a batch culture with no additional glutamine at the beginning.

The evolution of individual glycans strongly depends on the nucleotide sugar levels. For example, Fig. 6 compares the accumulated composition of F(6)A2G2, a dominant OS structure with two galactose, and F(6)A2G0, with no galactose, along the culture time. The F(6)A2G2 availability diminishes along the culture time. The steepest decline can be

seen from approximately the 3<sup>rd</sup> to the 5<sup>th</sup> day of the culture, which might be attributed to the glucose reduction exhibited in Fig. 4. On the contrary, an increase is observed in F(6)A2G0 abundance, supporting the dependency of OS structure on the extracellular metabolites. The model correctly predicted these trends.

Fig. 7 provides the time profile of accumulated GI in the culture, illustrating the ability of the model to predict the trends in the index. As explained earlier, due to the consumption of glucose and glutamine, the nucleotide sugar concentration decline with culture time. This leads to an increase in the abundance of agalctosylated OSs and a relative decrease in digalactosylated OSs and hence, a decrease in GI.

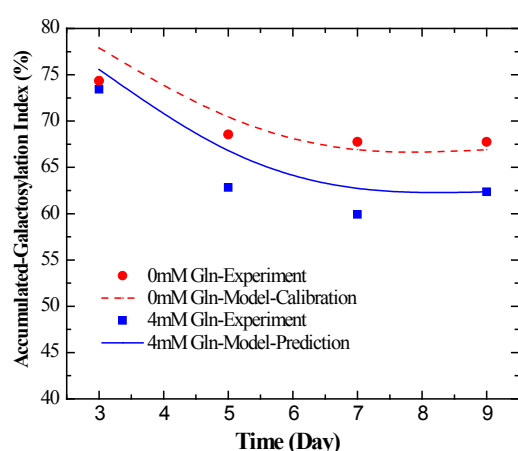


Fig. 7. Accumulated galactosylation index (GI) time profile of two distinguishable batch cultures. Red: calibration vs. experiment, Blue: prediction vs. experiment

As glucose depletes faster in the presence of glutamine (squares in Fig. 7), the accumulated GI for the culture commenced with initial 4mM glutamine lies beneath the one with no glutamine. The dashed line shows the calibration quality of the model for the GI of culture with no initial glutamine, while the solid line depicts the prediction capability of the model for forecasting the GI for the culture with initial glutamine concentration of 4mM. It is worth mentioning that the measurements of OSs and recombinant protein concentrations suffer from considerable experimental error, due to the large number of experimental steps required for analysis.

## 5. CONCLUSIONS

The dynamic metabolic flux model provided an adequate approximation of the extracellular metabolite concentrations, assuming glucose and glutamine co-metabolism. The parameters of this model were calibrated using experimental results for the culture with 4 mM glutamine presented initially and validated by comparing the simulation results with experimental results of the culture with an initial glutamine concentration of zero. The production of nucleotide sugars in the cytosol (or nucleus) as a function of extracellular glucose and glutamine concentrations were

formulated. This model plays a crucial role in linking the glycosylation pattern of Mab to the corresponding extracellular culture conditions. Ultimately, the glycosylation of Mab inside the Golgi apparatus has also been formulated based on the Golgi maturation hypothesis and successfully linked to the above mentioned models. Additionally, for comparing the model predictions to experiments, an averaging calculation was implemented to convert instantaneous glycoprofiles within the cell to accumulated ones. The model correctly predicted dynamic trends in glycosylation indices as well as specific glycan species.

## REFERENCES

- Brockhausen, I. (2006). *Glycobiology protocols*, Totowa, N.J., Humana ; Arkholme : Quantum [distributor].
- Burnham, K. P. & Anderson, D. R. (2002). *Model selection and multi-model inference : a practical information-theoretic approach*, New York ; London, Springer.
- Del Val, I. J., Nagy, J. M. & Kontoravdi, C. (2011). A dynamic mathematical model for monoclonal antibody N-linked glycosylation and nucleotide sugar donor transport within a maturing Golgi apparatus. *Biotechnology Progress*, 27, 1730-1743.
- Durocher, Y. & Butler, M. (2009). Expression systems for therapeutic glycoprotein production. *Current Opinion in Biotechnology*, 20, 700-707.
- Hossler, P., Khattak, S. F. & Li, Z. J. (2009). Optimal and consistent protein glycosylation in mammalian cell culture. *Glycobiology*, 19, 936-949.
- Hossler, P., Mulukutla, B. C. & Hu, W. S. (2007). Systems Analysis of N-Glycan Processing in Mammalian Cells. *Plos One*, 2.
- Jitjareonchai, J. J., Reilly, P. M., Duever, T. A. & Chambers, D. B. (2006). Parameter estimation in the Error-in-Variables models using the Gibbs Sampler. *Canadian Journal of Chemical Engineering*, 84, 125-138.
- Kanehisa, M. & Goto, S. (2000). KEGG: Kyoto Encyclopedia of Genes and Genomes. *Nucleic Acids Research*, 28, 27-30.
- Kanehisa, M., Goto, S., Sato, Y., Furumichi, M. & Tanabe, M. (2012). KEGG for integration and interpretation of large-scale molecular data sets. *Nucleic Acids Research*, 40, D109-D114.
- Majid, F. a. A., Butler, M. & Al-Rubeai, M. (2007). Glycosylation of an immunoglobulin produced from a murine hybridoma cell line: The effect of culture mode and the anti-apoptotic gene, bcl-2. *Biotechnology and Bioengineering*, 97, 156-169.
- Naderi, S., Meshram, M., Wei, C., Mcconkey, B., Ingalls, B., Budman, H. & Scharer, J. (2011). Development of a Mathematical Model for Evaluating the Dynamics of Normal and Apoptotic Chinese Hamster Ovary Cells. *Biotechnology Progress*, 27, 1197-1205.
- Stanley, P. (2011). Golgi Glycosylation. *Cold Spring Harbor Perspectives in Biology*, 3.